in one direction. This is the case, for example, in our experimental verification in a single-mode waveguide system. A similar behavior can be obtained with 3D bodies with a high-aspect ratio, where the field along one axis asymptotically becomes uniform [see fig. S15 (*25*)]. We believe that it provides a new pathway to engineer electromagnetic metamaterials and structures with near-zero parameters, as well as their associated photonic phenomena. Specific examples of the potential scientific and technological applications of this concept might include reconfigurable and flexible photonics (with a single small actuator that is arbitrarily located), nonlinear optics (with enhanced field penetration in the ENZ host), and quantum metamaterials.

REFERENCES AND NOTES

1. S. M. Sze, K. N. Kwok, *Physics of Semiconductor Devices* (Wiley, ed. 3, 2006).
2. A. S. Sedra, K. C. Smith, *Microelectronic Circuits* (Oxford Univ. Press, 1998).
3. P. Würfel, U. Würfel, *Physics of Solar Cells: From Basic Principles to Advance Concepts* (Wiley-VCH, ed. 3, 2016).
4. S. C. Erwin *et al.*, *Nature* **436**, 91–94 (2005).
5. N. Engheta, R. W. Ziolkowski, *Metamaterials: Physics and Engineering Explorations* (IEEE-Wiley, 2006).
6. G. V. Eleftheriades, K. G. Balmain, *Negative-Refraction Metamaterials: Fundamental Principles and Applications* (Wiley, 2005).
7. R. W. Ziolkowski, *Phys. Rev. E* **70**, 046608 (2004).
8. M. Silveirinha, N. Engheta, *Phys. Rev. Lett.* **97**, 157403 (2006).
9. M. G. Silveirinha, N. Engheta, *Phys. Rev. B* **75**, 075119 (2007).
10. A. H. Sihvola, *Electromagnetic Mixing Formulas and Applications* (IET, 1999).
11. Y. Wu, J. Li, Z. Q. Zhang, C. T. Chan, *Phys. Rev. B* **74**, 085111 (2006).
12. A. Alù, *Phys. Rev. B* **84**, 075153 (2011).
13. P. M. T. Ikonen, E. Saenz, R. Gonzalo, C. R. Simovski, S. A. Tretyakov, *Metamaterials* **1**, 89–105 (2007).
14. M. G. Silveirinha, N. Engheta, *Phys. Rev. B* **76**, 245109 (2007).
15. B. Edwards, A. Alù, M. E. Young, M. Silveirinha, N. Engheta, *Phys. Rev. Lett.* **100**, 033903 (2008).
16. I. Liberal, A. M. Mahmoud, N. Engheta, *Nat. Commun.* **7**, 10989 (2016).
17. S. Enoch, G. Tayeb, P. Sabouroux, N. Guérin, P. Vincent, *Phys. Rev. Lett.* **89**, 213902 (2002).
18. R. Sokhoyan, H. A. Atwater, *Opt. Express* **21**, 32279–32290 (2013).
19. M. Z. Alam, I. De Leon, R. W. Boyd, *Science* **352**, 795–797 (2016).
20. L. Caspani *et al.*, *Phys. Rev. Lett.* **116**, 233901 (2016).
21. A. Capretti, Y. Wang, N. Engheta, L. Dal Negro, *Opt. Lett.* **40**, 1500–1503 (2015).
22. M. G. Silveirinha, *Phys. Rev. A* **89**, 023813 (2014).
23. F. Monticone, A. Alù, *Phys. Rev. Lett.* **112**, 213903 (2014).
24. I. Liberal, N. Engheta, *Sci. Adv.* **2**, e1600987 (2016).
25. See supplementary materials.
26. D. Sievenpiper, Z. Lijun, R. F. J. Broas, N. G. Alexopoulos, E. Yablonovitch, *IEEE Trans. Microw. Theory Tech.* **47**, 2059–2074 (1999).
27. A. M. Mahmoud, N. Engheta, *Nat. Commun.* **5**, 5638 (2014).
28. V. C. Nguyen, L. Chen, K. Halterman, *Phys. Rev. Lett.* **105**, 233908 (2010).
29. C. Della Giovampaola, N. Engheta, *Phys. Rev. B* **93**, 195152 (2016).
30. The numerical calculations were all performed in COMSOL Multiphysics 5.0 (available at www.comsol.com).

ACKNOWLEDGMENTS

We acknowledge partial support from the Vannevar Bush Faculty Fellowship program, sponsored by the Basic Research Office of the Assistant Secretary of Defense for Research and Engineering and funded by the Office of Naval Research through grant N00014-16-1-2029, and partial support from the U.S. Air Force Office of Scientific Research Multidisciplinary University Research Initiative Awards FA9550-12-1-0488 and FA9550-14-1-0389. Y.L. acknowledges partial support from the National Natural Science Foundation of China under grant 61301001. All data used to obtain our conclusions are present in the main paper and/or the supplementary materials. Additional data related to this paper may be requested from N.E.

SUPPLEMENTARY MATERIALS

www.sciencemag.org/content/355/6329/1058/suppl/DC1
Supplementary Text
Figs. S1 to S15
References (*31*–*33*)

23 October 2016; accepted 13 February 2017
10.1126/science.aal2672

OPTICAL METAMATERIALS

Scalable-manufactured randomized glass-polymer hybrid metamaterial for daytime radiative cooling

Yao Zhai,[1]* Yaoguang Ma,[1]* Sabrina N. David,[2] Dongliang Zhao,[1] Runnan Lou,[3] Gang Tan,[4] Ronggui Yang,[1]† Xiaobo Yin[1,2]†

Passive radiative cooling draws heat from surfaces and radiates it into space as infrared radiation to which the atmosphere is transparent. However, the energy density mismatch between solar irradiance and the low infrared radiation flux from a near-ambient-temperature surface requires materials that strongly emit thermal energy and barely absorb sunlight. We embedded resonant polar dielectric microspheres randomly in a polymeric matrix, resulting in a metamaterial that is fully transparent to the solar spectrum while having an infrared emissivity greater than 0.93 across the atmospheric window. When backed with a silver coating, the metamaterial shows a noontime radiative cooling power of 93 watts per square meter under direct sunshine. More critically, we demonstrated high-throughput, economical roll-to-roll manufacturing of the metamaterial, which is vital for promoting radiative cooling as a viable energy technology.

Radiative cooling—deposition of blackbody radiation from a hot object through the infrared transparency window of the atmosphere to the cold sink of outer space—is an appealing concept for the 21st century, when most daily necessities, from power generation to data centers, generate excess heat. In contrast to most of the currently used cooling methods that require energy and resources to carry heat away, radiative cooling is a passive enhancement of Earth's natural method of cooling itself. Efficient nighttime radiative cooling systems have been extensively investigated in the past, with promising infrared emissivity in both organic and inorganic materials, including pigmented paints (*1*–*5*). Daytime radiative cooling, however, presents a different challenge because solar absorbance of just a few percent exceeds the cooling power and effectively heats the surface. Recently proposed nanophotonic devices can effectively reject solar irradiance but emit strongly in infrared (*6*, *7*), which is promising for daytime radiative cooling. However, the nanophotonic approach requires stringent, nanometer-precision fabrication, which is difficult to scale up cost-effectively in order to meet the large area requirements of the residential and commercial applications that can benefit most from radiative cooling.

Polymeric photonics is a growing field and attractive for economy and scalability (*8*–*11*). Hybridization of random optical metamaterials with polymer photonics can be a promising approach for efficient daytime radiative cooling; to date, harnessing randomness in photonic systems has yielded amplified spontaneous emission (*12*, *13*), extremely localized electromagnetic hot spots (*14*–*16*), improved light-trapping efficiency of photovoltaic cells (*17*, *18*), and negative permeability and switching devices with multistability (*19*, *20*). When electromagnetic resonators in a random metamaterial are collectively excited, the extinction and the optical path length in the material are both enhanced, resulting in nearly perfect absorption at the resonance (*21*, *22*). This implies great potential for using metamaterials with randomly distributed optical resonators for effective radiative cooling, if perfect absorption (emissivity) across the entire atmospheric transmission window can be achieved.

Here, we demonstrate efficient day- and nighttime radiative cooling with a randomized, glass-polymer hybrid metamaterial. The metamaterial consists of a visibly transparent polymer encapsulating randomly distributed silicon dioxide (SiO_2) microspheres. The spectroscopic response spans two orders of magnitude in wavelength (0.3 to 25 μm). Our hybrid metamaterial is extremely emissive across the entire atmospheric transmission window (8 to 13 μm) because of the phonon-enhanced Fröhlich resonances of the microspheres. A 50-μm-thick metamaterial film containing 6% of microspheres by volume has an averaged infrared emissivity of >0.93 and reflects ~96% of solar irradiance when backed with a 200-nm-thick silver coating. We experimentally demonstrate an average noontime (11 a.m. to 2 p.m.) radiative cooling power of 93 W/m^2 under direct sunshine during a 3-day field test and an average cooling power of >110 W/m^2 over the continuous 72-hour day-and-night test. The metamaterial was fabricated in 300-mm-wide sheets at a rate of 5 m/min, so that in the course of the experiment, we produced hundreds of square meters of the material.

The proposed structure of the randomized, glass-polymer hybrid metamaterial contains micrometer-sized SiO_2 spheres randomly distributed in a matrix material of polymethylpentene (TPX) (Fig. 1A). We used TPX because of its excellent solar transmittance. Other visibly transparent polymers such as poly(methyl methacrylate) and polyethylene can be used but would slightly increase solar absorption. Because both the polymer matrix material and the encapsulated SiO_2 microspheres are lossless in the solar spectrum, absorption is nearly absent, and direct solar irradiance does not heat the metamaterial.

At infrared wavelengths, the encapsulated SiO_2 microspheres have optical properties drastically different from that of the surrounding matrix material, owing to the existence of strong phonon-polariton resonances at 9.7 μm (*23*). We calculated the normalized absorbance (σ_{abs}/a^2), scattering (σ_{sca}/a^2), and extinction (σ_{ext}/a^2) cross sections of an individual microsphere encapsulated in TPX as a function of its size parameter, k_0a, for an incident wavelength of 10 μm (Fig. 1B). Here, k_0 is the wave vector in free space, and a is the radius of the microsphere. The extinction peaks at a size parameter of ~2.5, corresponding to a microsphere radius of ~4 μm. The size parameter of the microsphere plays a key role in designing the hybrid metamaterial for radiative cooling. At the small particle (quasi-static) limit, the resonance is purely electric-dipolar in character (Fig. 1B, inset). At the extinction peak, high-order Fröhlich resonances, including both electric and magnetic modes, are also strongly excited, which is evidenced by the strong forward scattering shown in Fig. 1C, the three-dimensional power scattering function (far-field scattering pattern) (*24*).

The intrinsically narrow linewidth of phonon polaritons—often a superior advantage in applications such as infrared sensing (*25*, *26*)—can here limit the bandwidth of the highly emissive infrared region. We obtained broadband emissivity across the entire atmospheric window by

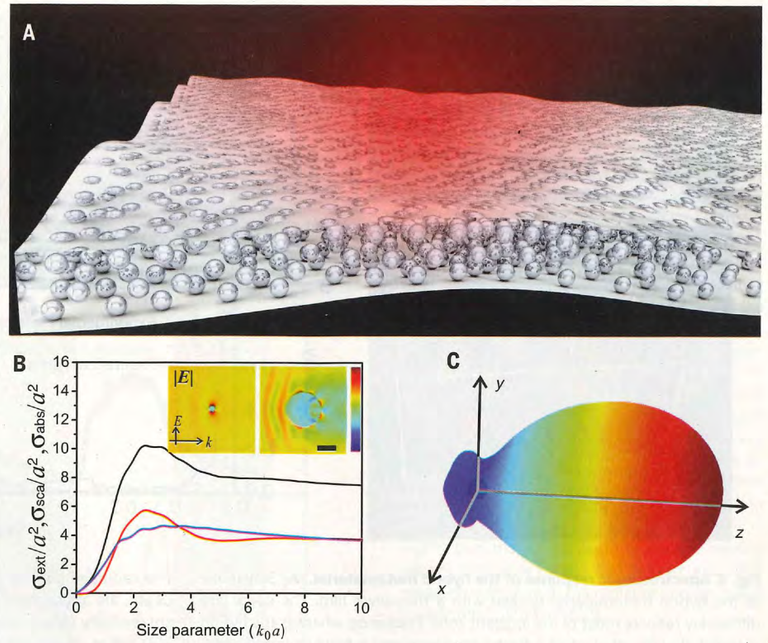

Fig. 1. Glass-polymer hybrid metamaterial. (**A**) A schematic of the polymer-based hybrid metamaterial with randomly distributed SiO_2 microsphere inclusions for large-scale radiative cooling. The polarizable microspheres interact strongly with infrared light, making the metamaterial extremely emissive across the full atmospheric transmission window while remaining transparent to the solar spectrum. (**B**) Normalized absorption (blue), scattering (red), and extinction (black) cross sections of individual microspheres as functions of size parameter (k_0a). The extinction—the sum of the scattering and absorption—peaks at a size parameter of 2.5, which corresponds to a microsphere radius of 4 μm. (Inset) The electric field distributions of two microspheres with 1- and 8-μm diameters, illuminated at a 10-μm wavelength. Scale bar, 4 μm. The smaller microsphere resonates at the electric dipolar resonance, whereas higher-order electric and magnetic modes are excited in the larger microsphere. (**C**) Angular diagram for the scattering far-field irradiance of an 8-μm-diameter microsphere with 10-μm wavelength illumination. The incident field is polarized along the *y* direction and propagating along the *z* direction.

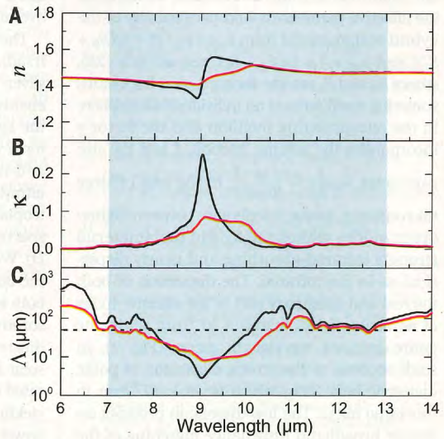

Fig. 2. Fröhlich resonance and broadband infrared absorbance of the hybrid metamaterial. (**A** and **B**) The real (A) and imaginary (B) part of the effective index of refraction for the glass-polymer hybrid metamaterials. The metamaterial with 1-μm-diameter SiO_2 microspheres (black curves) shows a strong Fröhlich resonance at its phonon-polariton frequency of 9.7 μm, whereas the metamaterial with 8-μm-diameter microspheres (red curves) shows significantly more broadband absorption across infrared wavelengths. The strong Fröhlich resonance not only limits the bandwidth of strong emissivity but also introduces strong reflectance of incident infrared radiation. In both cases, the metamaterial contains 6% SiO_2 by volume. (**C**) The attenuation lengths of the two hybrid metamaterials, with the 8-μm-diameter SiO_2 microsphere case showing an average attenuation length of ~50 μm from λ = 7 to 13 μm.

[1]Department of Mechanical Engineering, University of Colorado, Boulder, CO 80309, USA. [2]Materials Science and Engineering Program, University of Colorado, Boulder, CO 80309, USA. [3]Department of Aerospace Engineering Sciences, University of Colorado, Boulder, CO 80309, USA. [4]Department of Civil and Architectural Engineering, University of Wyoming, Laramie, WY 82071, USA.
*These authors contributed equally to this work. †Corresponding author. Email: xiaobo.yin@colorado.edu (X.Y); ronggui.yang@colorado.edu (R.Y.)

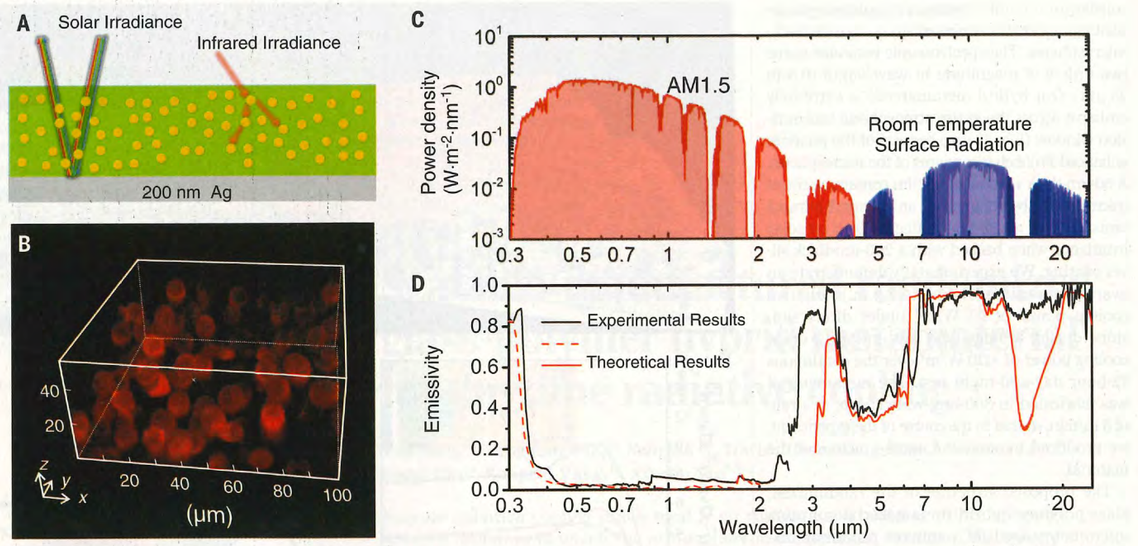

Fig. 3. Spectroscopic response of the hybrid metamaterial. (**A**) Schematic of the hybrid metamaterial backed with a thin silver film. The silver film diffusively reflects most of the incident solar irradiance, whereas the hybrid material absorbs all incident infrared irradiance and is highly infrared emissive. (**B**) Three-dimensional confocal microscope image of the hybrid metamaterial. The microspheres are visible because of the autofluorescence of SiO_2. (**C**) Power density of spectral solar irradiance [air mass (AM) 1.5] and thermal radiation of a blackbody at room temperature. The sharply varying features of both spectra are due to the absorbance of the atmosphere. The radiative cooling process relies on strong emission between 8 and 13 μm, the atmospheric transmission window. (**D**) The measured emissivity/absorptivity (black curve) of the 50-μm-thick hybrid metamaterial from 300 nm to 25 μm. Integrating spheres are used for the measurement of both solar (300 nm to 2.5 μm) and infrared (2.5 to 25 μm) spectra. Theoretical results for the same hybrid metamaterial structure (red curves) are plotted for comparison. Two different numerical techniques, RCWA and incoherent transfer matrix methods, are used for the solar and infrared spectral ranges, respectively.

accessing the high-order Fröhlich resonances of the polar dielectric microspheres (*27*). The real and the imaginary parts of the extracted effective index of refraction, $n + i\kappa = \sqrt{\varepsilon_{eff} \cdot \mu_{eff}}$, are functions of wavelength and microsphere sizes, as illustrated in Fig. 2 for 1- and 8-μm-diameter microspheres. Given the low concentration (6% by volume) and assuming that the microspheres are uniform in size and distribution, we retrieved the effective permittivity and permeability of the hybrid metamaterial from $\varepsilon_{eff} = \varepsilon_p \cdot [1 + i\gamma(S_0 + S_1)]$ and $\mu_{eff} = 1 + i\gamma(S_0 + S_1)$, respectively (*28*), where S_0 and S_1 are the forward- and backward-scattering coefficients of an individual microsphere in the encapsulating medium and the factor γ incorporates the volume fraction, *f*, and the size parameter, $k_0 a \left[\gamma = \frac{3f}{2(k_0 a)^3}\right]$. In the case of large microspheres, modal interference between higher-order modes makes the hybrid metamaterial strongly infrared-absorbing and nearly dispersionless in the infrared. The dispersion of both the real and imaginary part of the effective index of refraction is less than 9×10^{-5}/nm across the entire infrared wavelength range (Fig. 2), in stark contrast to the strong dispersion of polar, dielectric bulk SiO_2, which is $\sim 5 \times 10^{-3}$/nm in this same range. The low dispersion provides excellent broadband impedance matching of the metamaterial to free space, resulting in extremely low reflectance for both solar and infrared radiation. A hybrid metamaterial as thin as 50 μm can provide uniform and sufficiently strong absorbance across the entire atmospheric window, resulting in perfect broadband infrared emission for radiative cooling (Fig. 2C). In contrast, when the microspheres are small ($k_0 a << 1$), a sharp resonance occurs (Fig. 2B), which limits the high infrared emissivity to the polariton resonance wavelength only. Moreover, the resonance introduces strong reflectance, further reducing the overall emissivity.

The hybrid metamaterial strongly reflects solar irradiation when backed with a 200-nm-thick silver thin film (Fig. 3A) prepared by means of electron beam evaporation. We characterized the spectroscopic performance of the metamaterial thin film in both the solar (0.3 to 2.5 μm) and infrared (2.5 to 25 μm) regions using an ultraviolet-visible–near-infrared (UV-Vis-NIR) spectrophotometer and Fourier transform infrared spectrometer (FTIR), respectively (Fig. 3, C and D). We used integrating spheres to account for the scattered light from the full solid angle in both spectral regions. The measured spectral absorptivity (emissivity) of the sample (Fig. 3D) indicates that the 50-μm-thick film reflects ~96% solar irradiation while possessing a nearly saturated emissivity of >0.93 between 8 and 13 μm—yielding greater than 100 W/m^2 radiative cooling power under direct sunlight at room temperature. The experimental results agree well with theory, in which the spectroscopic discrepancies near 3- and 16-μm wavelengths are primarily due to the absorbance of water and air during the FTIR measurement in ambient conditions. We must use different theoretical approaches for calculating the emissivity in the solar and infrared wavelength ranges. We used the generalized, incoherent transfer-matrix method in the infrared region (*29*). In the solar region, we instead used rigorous coupled wave analysis (RCWA) because the extracted effective parameters of the metamaterial are inaccurate when the size of the microsphere is greater than the relevant wavelengths (*30*). The high emissivity in the second atmospheric window between 16 and 25 μm might be harnessed for additional radiative cooling (*31*).

Using a polymer as the matrix material for radiative cooling has the advantages of being lightweight and easy to laminate on curved surfaces. It can accommodate small variations in microsphere size and shape, with negligible impact on the overall performance. TPX has excellent mechanical and chemical resistance, offering potentially long lifetimes for outdoor use. However, one of the most compelling advantages of developing a glass-polymer hybrid metamaterial lies in the possibility of cost-effective scalable fabrication. We produced a roll of 300-mm-wide and 50-μm-thick hybrid metamaterial film at a rate of 5 m/min (Fig. 4A). We controlled the volume concentration of the SiO_2 microspheres by using gravimetric feeders. The resultant film has a homogeneous distribution of microspheres,

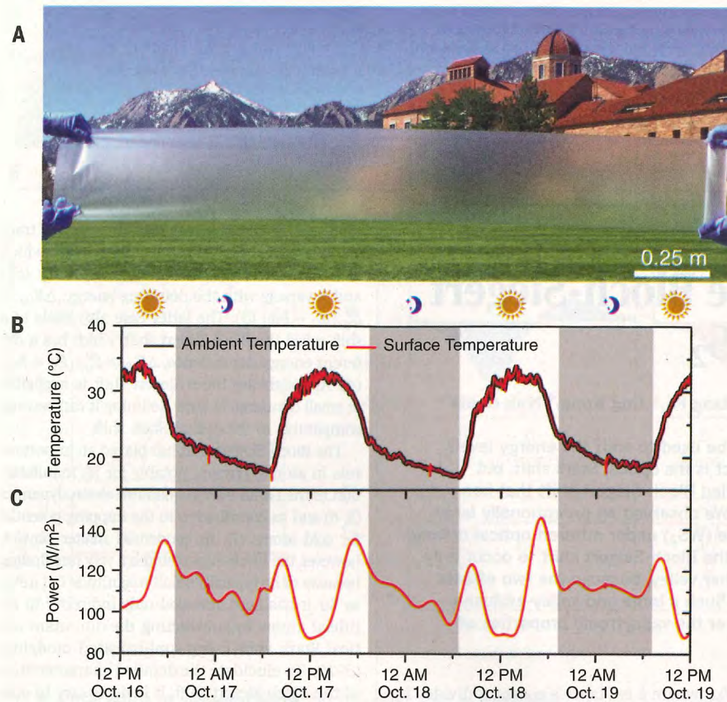

Fig. 4. Performance of scalable hybrid metamaterial for effective radiative cooling. (**A**) A photo showing the 300-mm-wide hybrid metamaterial thin film that was produced in a roll-to-roll manner, at a speed of 5 m/min. The film is 50 μm in thickness and not yet coated with silver. (**B**) A 72-hour continuous measurement of the ambient temperature (black) and the surface temperature (red) of an 8-in-diameter hybrid metamaterial under direct thermal testing. A feedback-controlled electric heater keeps the difference between ambient and metamaterial surface temperatures less than 0.2°C over the consecutive 3 days. The heating power generated by the electric heater offsets the radiative cooling power from the hybrid metamaterial. When the metamaterial has the same temperature as the ambient air, the electric heating power precisely measures the radiative cooling power of the metamaterial. The shaded regions represent nighttime hours. (**C**) The continuous measurement of radiative cooling power over 3 days shows an average cooling power of >110 W/m^2 and a noontime cooling power of 93 W/m^2 between 11 a.m. and 2 p.m. The average nighttime cooling power is higher than that of the daytime, and the cooling power peaks after sunrise and before sunset. The measurement error of the radiative cooling power is well within 10 W/m^2 (*32*).

with fluctuations in concentration of less than 0.4% (fig. S1) (*32*). The hybrid metamaterial films are translucent because of the scattering of visible light from the microsphere inclusions (fig. S2) (*32*). Additionally, when backed with a 200-nm-thick reflective silver coating, the hybrid metamaterial has a balanced white color (fig. S2) (*32*). The strongly scattering and nonspecular optical response of the metamaterial will avoid back-reflected glare, which can have detrimental visual effects for humans and interfere with aircraft operations (*33*).

We demonstrated real-time, continuous radiative cooling by conducting thermal measurements using an 8-in-diameter, scalably fabricated hybrid metamaterial film over a series of clear autumn days in Cave Creek, Arizona (33°49′32″N, 112°1′44″W, 585 m altitude) (Fig. 4, B and C). The metamaterial was placed in a foam container that prevents heat loss from below. The top surface of the metamaterial faced the sky and was directly exposed to the air (fig. S3) (*32*). We kept the surface temperature of the metamaterial the same as the measured ambient temperature using a feedback-controlled electric heater placed in thermal contact with the metamaterial so as to minimize the impacts of conductive and convective heat losses. The total radiative cooling power is therefore the same as the heating power generated by the electric heater if there is no temperature difference between the surface and the ambient air. With the feedback control, the surface temperature follows the measured ambient temperature within ±0.2°C accuracy during the day and less than ±0.1°C at night (fig. S4) (*32*). We continuously measured radiative cooling power, which gives an average radiative cooling power of >110 W/m^2 over a continuous 72-hour day- and nighttime measurement (Fig. 4C). The average cooling power around noon reaches 93 W/m^2, with normal-incidence solar irradiance greater than 900 W/m^2. We observed higher average nighttime radiative cooling than during the day. However, the cooling power peaks after sunrise and before sunset, when the ambient temperature is changing rapidly and solar irradiance is incident at large oblique angles. To further demonstrate the effectiveness of radiative cooling, we also used water as a cold storage medium and show cold water production with the scalably fabricated hybrid metamaterial (fig. S6) (*32*). Although we did not determine the reliability and lifetime of the glass-polymer hybrid metamaterials for outdoor applications, applying chemical additives and high-quality barrier coatings may enhance their outdoor performance. Many polymeric thin films are currently available and designed with extended outdoor lifetimes (*34*).

REFERENCES AND NOTES

1. S. Catalanotti *et al.*, *Sol. Energy* **17**, 83–89 (1975).
2. C. G. Granqvist, A. Hjortsberg, *J. Appl. Phys.* **52**, 4205–4220 (1981).
3. B. Orel, M. Klanjšek Gunde, A. Krainer, *Sol. Energy* **50**, 477–482 (1993).
4. A. R. Gentle, G. B. Smith, *Adv. Sci. (Weinh.)* **2**, 1500119 (2015).
5. M. M. Hossain, M. Gu, *Adv. Sci. (Weinh.)* **3**, 1500360 (2016).
6. E. Rephaeli, A. Raman, S. Fan, *Nano Lett.* **13**, 1457–1461 (2013).
7. A. P. Raman, M. A. Anoma, L. Zhu, E. Rephaeli, S. Fan, *Nature* **515**, 540–544 (2014).
8. M. F. Weber, C. A. Stover, L. R. Gilbert, T. J. Nevitt, A. J. Ouderkirk, *Science* **287**, 2451–2456 (2000).
9. S. D. Hart *et al.*, *Science* **296**, 510–513 (2002).
10. J. K. Gansel *et al.*, *Science* **325**, 1513–1515 (2009).
11. R. D. Rasberry *et al.*, *J. Mater. Chem.* **21**, 13902 (2011).
12. H. E. Türeci, L. Ge, S. Rotter, A. D. Stone, *Science* **320**, 643–646 (2008).
13. D. S. Wiersma, *Nat. Phys.* **4**, 359–367 (2008).
14. S. Grésillon *et al.*, *Phys. Rev. Lett.* **82**, 4520–4523 (1999).
15. L. Sapienza *et al.*, *Science* **327**, 1352–1355 (2010).
16. M. Segev, Y. Silberberg, D. N. Christodoulides, *Nat. Photonics* **7**, 197–204 (2013).
17. E. Yablonovitch, *J. Opt. Soc. Am.* **72**, 899 (1982).
18. H. A. Atwater, A. Polman, *Nat. Mater.* **9**, 205–213 (2010).
19. B. J. Seo, T. Ueda, T. Itoh, H. Fetterman, *Appl. Phys. Lett.* **88**, 161122 (2006).
20. P. Jung *et al.*, *Nat. Commun.* **5**, 3730 (2014).
21. X. Shen *et al.*, *Appl. Phys. Lett.* **101**, 154102 (2012).
22. J. Hao, É. Lheurette, L. Burgnies, É. Okada, D. Lippens, *Appl. Phys. Lett.* **105**, 081102 (2014).
23. E. D. Palik, *Handbook of Optical Constants of Solids* (Academic, 1985)
24. W. Liu *et al.*, *Opt. Express* **22**, 16178–16187 (2014).
25. N. Ocelic, R. Hillenbrand, *Nat. Mater.* **3**, 606–609 (2004).
26. I. Balin, N. Dahan, V. Kleiner, E. Hasman, *Appl. Phys. Lett.* **94**, 111112 (2009).
27. Y. Zhao, M. A. Belkin, A. Alù, *Nat. Commun.* **3**, 870 (2012).
28. M. S. Wheeler, J. S. Aitchison, J. I. Chen, G. A. Ozin, M. Mojahedi, *Phys. Rev. B* **79**, 073103 (2009).
29. C. C. Katsidis, D. I. Siapkas, *Appl. Opt.* **41**, 3978–3987 (2002).
30. L. F. Li, *J. Opt. Soc. Am. A Opt. Image Sci. Vis.* **13**, 1870 (1996).
31. H. W. Yates, J. H. Taylor, "Infrared transmission of the atmosphere," no. NRL-5453 (Naval Research Lab, 1960).
32. Materials and methods are available as supplementary materials.
33. X. Xu, K. Vignarooban, B. Xu, K. Hsu, A. M. Kannan, *Renew. Sustain. Energy Rev.* **53**, 1106–1131 (2016).
34. H. Price *et al.*, *J. Sol. Energy Eng.* **124**, 109 (2002).